Catal Lett (2012) 142:417–426
DOI 10.1007/s10562-012-0793-5

Bio *n*-Butanol Partial Oxidation to Butyraldehyde in Gas Phase on Supported Ru and Cu Catalysts

J. Requies · M. B. Güemez · A. Iriondo · V. L. Barrio · J. F. Cambra · P. L. Arias

Received: 18 November 2011 / Accepted: 29 February 2012 / Published online: 17 March 2012

Abstract Ceria, titania, and zirconia supported ruthenium and copper catalysts were tested in the butyraldehyde production by gas phase *n*-butanol partial oxidation. These catalysts were characterized by means of N_2 adsorption–desorption isotherms, temperature-programmed reduction and X-ray photoelectron spectroscopy techniques. The activity tests were performed in a fixed bed reactor at 0.1 MPa and 623 K using air and *n*-butanol mixture as reactants (in stoichiometric proportion *n*-butanol/O_2) to generate butyraldehyde. For *n*-butanol partial oxidation, the ruthenium catalysts showed higher activity and stability than the copper ones. The *n*-butanol conversion was almost similar for all the ruthenium catalysts, but the different supports modified the metal dispersion and, as a result, the product distribution was modified. The catalysts supported on ZrO_2 and CeO_2 allowed the highest butyraldehyde yields. The copper doping of the ruthenium catalyst also improved the selectivity toward butyraldehyde.

Keywords Environmental catalysis · Heterogeneous catalysis · Green chemistry

1 Introduction

Aldehydes are important organic molecules for the synthesis of many different high-added value products. There is an increasing interest in renewable sources for all type of chemicals. Bioalcohols, such as ethanol, butanol or glycerol can be obtained from biomass and can be converted to their corresponding aldehydes. Nevertheless, adequate processes are required for these conversions. Nowadays, industrial large-scale production of butyraldehyde takes place through hydroformylation (oxo-synthesis) reaction of propylene. This process uses metal (Co, Rh, Ru) hydridocarbonyls complexes as homogeneous catalysts [1] to obtain in aldehyde mixtures: butyraldehyde and isobutyraldehyde. The ratio between both products depends on operating conditions (2–50 MPa and 363–453 K) and the catalyst employed. Other processes for aldehydes production also use homogeneous catalysts. For example the process developed by Ruhrchemie/Rhône-Poulene [2] employing two phases (water/organic solvent). This process can be operated at 50 MPa of pressure compared to hydroformylation process, has the advantage of facilitating the separation of its homogeneous catalyst and optimizes energy consumption. Nevertheless, the Ruhrchemie/Rhône-Poulene and hydroformylation processes present important problems as waste production and product purification. Hence, the development of heterogeneous catalysis processes, operating at less severe operating conditions and minimizing waste production presents economic and environmental benefits. Therefore, new routes of saturated and unsaturated aldehydes production are under study.

One of the most promising routes for aldehyde production is selective alcohol catalytic oxidation. This process with environmentally benign oxidants has been developed in the recent years [3–5]. Nevertheless, in most of the cases, the alcohol oxidation takes place in liquid phase [6], but the presence of a solvent is usually necessary to promote this reaction [2, 3, 6]. The presence of this solvent generates additional problems to obtain a pure final

J. Requies (✉) · M. B. Güemez · A. Iriondo · V. L. Barrio · J. F. Cambra · P. L. Arias
Department of Chemical and Environmental Engineering, School of Engineering, UPV/EHU, Bilbao, Spain
e-mail: jesus.requies@ehu.es

product. Different catalysts have been used for the oxidation of alcohols in liquid phase, for example, Cu-base catalysts [7], Co-based [8, 9] and noble metal based catalysts such as Ru, Pd and Os, among others [10–12].

Even if several studies have been published about the aldehydes production from alcohols in the presence of noble and non noble metals in liquid phase, few studies have been published for processes operating in gas phase. Some authors have studied the dehydrogenation of *n*-butanol under different formulations of solid catalysts: Cu–Ba [13], Ru/Fe_2O_3 [14], and ZnO [15]. Parentis et al. [16] studied the dehydrogenation reaction of primary alcohols of low molecular weight (C_2–C_4) at low alcohol conversion over a Cr/SiO_2 catalyst reaching high selectivity toward the corresponding aldehyde. Besides, they found that when oxygen was fed to this dehydrogenation process the aldehyde selectivity was higher. However, these studies were carried out at very low space velocity and low partial pressure of alcohol.

The aim of this work is to provide and discuss new information about activity and characterization of ruthenium, copper and ruthenium–copper catalysts supported on different oxides (ZrO_2, CeO_2 and TiO_2) in the *n*-butanol gas-phase partial oxidation. Previous results [17] showed that higher activities and selectivities toward butyraldehyde were reached using ruthenium catalysts. Moreover, in processes operating in liquid phase some condensation products were observed (butyl butyrate, 4-heptanone, butyl ether, etc.), while in gas phase main by-products were CO_2, H_2, CH_4 and other saturated and unsaturated hydrocarbons. It is well known [1] that primary alcohols are oxidized not only up to their corresponding aldehydes, but to their corresponding acids or even to more oxidized species (see Fig. 1). However, at the operating conditions used in this work, the butyric acid was not detected. This would indicate a much lighter oxidation process.

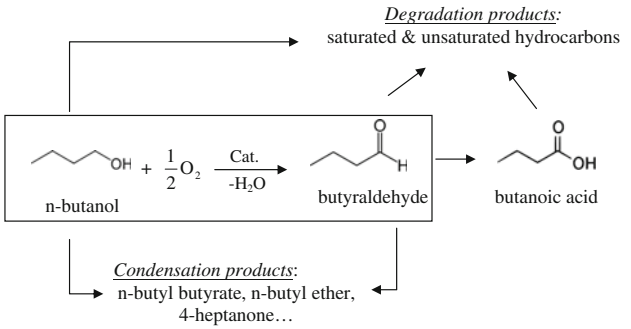

Fig. 1 Simplified scheme reaction of the catalytic partial oxidation of *n*-butanol

2 Experimental

2.1 Catalyst Preparation

Ruthenium, copper, and ruthenium-copper catalysts were prepared by the incipient wetness impregnation method. Support materials used were zirconium dioxide (ZrO_2 was obtained by calcination of zirconium hydroxide, kindly provided by Eurosupport, The Netherland), cerium dioxide (calcination of $Ce(NO_3)_3{\cdot}H_2O$ SigmaUltra >99.0 %, Sigma–Aldrich), and titanium dioxide (Degussa, Aeroxide titandioxide P25). $RuCl_3$ (Johnson Matthey, metallic base Ru 40 %) and $Cu(NO_3)_2{\cdot}3H_2O$ (Alfa Aesar, 98 %) salts were used as ruthenium and copper precursors, respectively. The monometallic catalysts: 5CuZr and 5CuTi (5 wt% nominal copper weight), 2RuZr, 2RuTi and 2RuCe (2 wt% nominal ruthenium), were prepared by a single-step impregnation. The preparation of bimetallic catalyst, designed as 2Ru5CuZr (2 wt% ruthenium and 5 wt% of copper nominal), was carried out by impregnation of the 5CuZr catalyst with ruthenium precursor solution. After impregnation and drying, the samples were calcined in air at 773 K for 2 h.

2.2 Catalysts Characterization

The catalysts were characterized by several physico-chemical techniques: plasma atomic emission spectroscopy (ICP-AES), surface area (BET method), temperature-programmed reduction (TPR) and X-ray photoelectron spectroscopy.

2.2.1 Plasma Atomic Emission Spectroscopy

Ruthenium and copper contents were determined by ICP-AES, using a Perkin-Elmer Optima 3300DV apparatus. Previous dissolution of the ground samples in acid solutions was required.

2.2.2 BET Surface Area

These measurements of the calcined catalysts were evaluated from the N_2 adsorption–desorption isotherms obtained at 77 K over the whole range of relative pressures, using a Micromeritics ASAP 2100 automatic device on samples previously degassed at 423 K for 24 h.

2.2.3 TPR Analysis

The temperature-programmed reduction was carried out using a Micromeritics TPD-TPR 2900 apparatus, equipped with a thermal conductivity detector. A continuous flow (40 NmL/min) of 10 % (v/v) H_2/Ar was passed over

200 mg of calcined catalyst powder. The temperature was increased from room temperature to 1,233 K at a rate of 10 K/min. The sample was previously outgassed at 523 K during 30 min.

2.2.4 XPS Analysis

These measurements were carried out with a VG Escalab 200R spectrometer equipped with a hemispherical electron analyser and an Al Kα1 ($h\nu = 1486.6$ eV, 1 eV = 1.6302×10^{19} J) 120 W X-ray source. The powdered samples were deposited on a stainless steel sample holder, placed in the pre-treatment chamber and degassed at 573 K. The spectra were collected at pass energy of 20 eV, which is typical of high-resolution conditions. Intensities were estimated by calculating the area of each peak, after smoothing, subtraction of the S-shaped background, and fitting the experimental curve to Lorentzian and Gaussian lines (20 % L/80 % G). Both fresh and used catalysts were analysed using this technique. Bonding energies reference was C 1*s*.

2.2.5 X-ray Diffraction (XRD)

XRD patterns were obtained using a Seifert XRD 3000P diffractometer, equipped with a PWBrag-Brentano u/2u 2200 goniometer, bent graphite monochromator and automatic slit, using a Cu Kα radiation ($\lambda = 0.15418$ nm) and 0.028° steps for scanning. Scherrer equation was used to estimate the particle average size of the crystalline species.

2.3 Activity Test

The activity tests were carried out in a bench-scale unit equipped with a tubular stainless steel reactor (1.15 cm i.d. and 30 cm length). The reactor was electrically heated in a furnace to the reaction temperature and a PID control was used to maintain the selected operation temperature constant. The effluent stream was cooled to room temperature and the gaseous and liquid products were separated. Prior to reaction, the catalysts were activated in situ with 100 NmL/min of 10 % (v/v) H_2/N_2 mixture at 0.1 MPa and 523 K during 2 h. The reduced catalysts were tested under the following conditions: 16.2 $g_{BuOH}\ g_{cat}^{-1}\ h^{-1}$, 0.1 MPa of total pressure and 623 K feeding 0.081 g/min of *n*-butanol (BuOH). The required molar flow of air was fed in order to obtain the stoichiometric molar ratio of *n*-butanol to oxygen ($BuOH/O_2 = 0.5$). To avoid temperature gradients in the catalytic bed, the catalyst (300 mg) was diluted with SiC at a 1:9 mass ratio. The particle size range was between 0.42 and 0.50 mm. The gas phase was on-line analyzed by a Micro GC Varian equipped with a high sensitivity TCD. Three columns: Molecular Sieve, Poraplot Q and CP-4900 were used in different modules for the complete gas separation. The liquid phase was analyzed by a GC (HP 6890) equipped with a FID and a TCD detectors and the column used was a DB-Wax. For a better understanding of catalytic activity and product distribution, the following parameters were calculated:

(i) *n*-butanol conversion:

$$\text{BuOH conv } (\%) = \frac{F_{\text{BuOH}}^{\text{Feed}} - F_{\text{BuOH}}^{\text{Out}}}{F_{\text{BuOH}}^{\text{Feed}}} \times 100 \quad (1)$$

(ii) Product yield:

$$Y(\%) = \frac{F_i^{\text{out}}}{F_{\text{BuOHconverted}}} \times 100 \quad (2)$$

where F_i are the moles of the compound "*i*" produced.

3 Results

3.1 Characterization Results

3.1.1 Chemical Composition and Characterization Textural

Table 1 shows the chemical composition of the catalysts prepared. It can be observed that for the monometallic catalysts, the load of copper was higher when ZrO_2 was used as support, followed by the loads obtained for the TiO_2 and CeO_2 supports, respectively. The higher metal copper loading was corresponding with higher BET surface. Similar behaviour was observed for ruthenium catalysts, but unfortunately, for the catalyst 2RuTi it was not possible to measure the metal content due to its incomplete disaggregation. Finally, the ruthenium–copper bimetallic catalyst presented lower metal contents than the corresponding monometallic catalysts.

The BET surface area, the total pore volume, and the average pore diameter (calculated using BJH method) are summarized in Table 2. For the zirconia-supported catalysts, the addition of the metallic phase, copper, copper–ruthenium or ruthenium, caused a severe decrease of BET area. This effect can be associated to pore blockage by metal incorporation and hence the specific surface area was reduced [18]. These data of surface area are in agreement with the micropore volume diminution and the rise of the average catalysts pore diameter (Table 2). The catalysts supported on ZrO_2 presented the highest microporosities, and no high differences were observed among them, whereas the Cu and Ru supported on cerium and titanium oxides catalysts showed higher mesoporosities. The incorporation of copper or ruthenium on the ceria support did not change significatively its textural characteristics.

Table 1 XPS results for fresh and used catalysts, M 2*p* or 3*d* is representing the different supports used in the studied reaction: Ce, Ti, or Zr

Catalysts	M 2*p* (3*d*)	Ru $3d_{5/2}$	Ru $3p_{3/2}$	Cu $2p_{3/2}$	Ru/M at	Cu/M at	ICP-AES (M wt%)
5CuZr fresh	182.2	–		934.0	–	0.11 (0.128)	6.18
5CuZr used	182.2	–		932.5 (40) 934.2 (60)	–	0.08	
5CuTi fresh	458.6	–		933.9	–	0.27 (0.073)	5.40
5CuTi used	–	–		–	–	–	
2RuZr fresh	182.2	282.1 (61) 283.0 (39)		–	0.06 (0.02)	–	1.26
2RuZr used	–		462.3 (69) 466.0 (31)	–	0.04	–	
2RuTi fresh	458.7	280.4 (66) 282.2 (34)		–	0.03	–	n.d.
2RuTi used	458.9	280.1		–	0.005	–	
2RuCe fresh	882.5	281.2 (65) 282.8 (35)		–	0.05	–	0.90
2RuCe used					0.008		
2Ru5CuZr fresh	182.1	281.0 (66) 282.9 (34)		934.2	0.1 (0.013)	0.19 (0.10)	0.99 (Ru)
2Ru5CuZr used	182.1 (80) 180.1 (20)		458.5 (67) 462.6 (33)	933.7 (37) 936.2 (63)	0.04	0.32	4.73 (Cu)

Theoretical bulk ratio (Cu/M or Ru/M) in parenthesis

Table 2 Physical and textural properties of the catalysts

Catalysts	BET surface area (m^2/g)	Total pore volume (cm^3/g)	Micropore volume (cm^3/g)	Average pore diameter (A)
ZrO_2	391.8	0.23	0.10	23.1
5CuZr	171.8	0.12	0.02	42.3
2RuZr	168.9	0.12	0.01	44.8
2Ru5CuZr	161.6	0.11	0.02	48.6
TiO_2	66.6	0.15	0.04	87.8
5CuTi	59.2	0.14	0.002	134.3
2RuTi	44.7	0.08	0.013	93.7
CeO_2	57.4	0.10	0.002	137.2
5CuCe	56.0	0.10	–	70.3
2RuCe	55.3	0.10	–	279.2

However, both the surface area and pore volume decreased when ruthenium was incorporated on the titania supports. This effect was much lower when copper is the metal incorporated; this can be attributed to bigger copper particles diameter.

3.1.2 TPR Results

The TPR profiles for the calcined catalysts at 773 K are showed in Figs. 2 and 3. For monometallic ruthenium catalysts on different supports, three peaks of reduction were observed in the range between 381 and 462 K. These peaks can be associated to ruthenium oxide reduction with different interaction with the support [19–21]. The ruthenium oxidation can be associated to the calcination treatment under airflow. According to several authors [20, 21] after this treatment, the ruthenium would be mainly in the RuO_2 form. This phenomenon was observed for several ruthenium catalysts as Ru/SiO_2, Ru/Al_2O_3, Ru/TiO_2 [20] and Ru/CeO_2 [21] catalysts. For monometallic copper catalysts, two reduction peaks were observed in the range between 395 and 472 K. These peaks can be associated to different copper oxide species interaction with the support. The less intense TPR peak can be attributed to fine copper particles well dispersed, while the most intense peak can be associated with larger copper oxide particles [22]. For the catalysts supported on ceria, two additional reduction peaks were observed that can be attributed to the reduction of superficial (at 720–729 K) and bulk CeO_2 (at 1005–1010 K) [22]. Similarly, the peaks centered at 710 and 861 K showed by the catalysts supported on zirconia can be associated to the reduction of zirconia [23].

For the bimetallic catalyst (2Ru5CuZr), only two reduction peaks were observed. These peaks correspond to the reduction peaks of Ru and Cu oxides. In this case, the highest peak associated to copper reduction is slightly shifted to lower temperatures as compared to the same peak

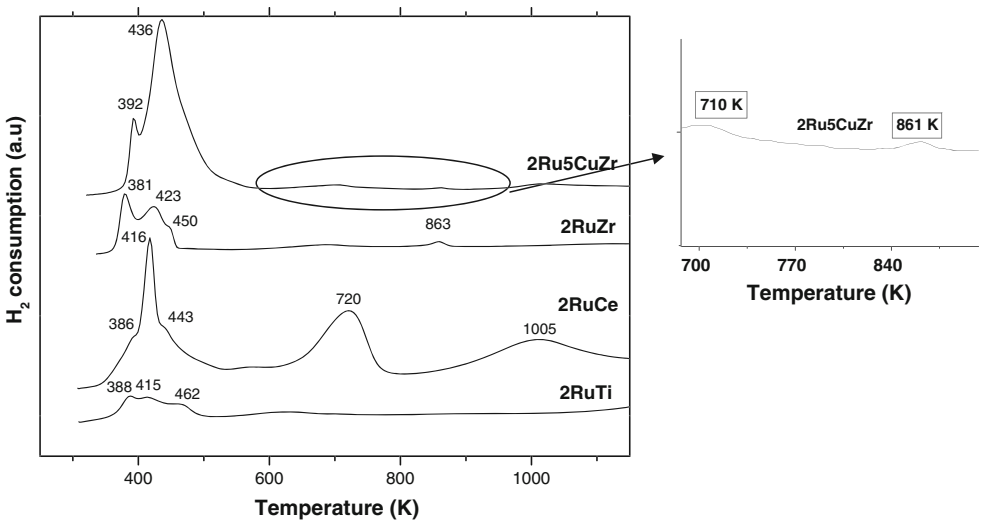

Fig. 2 TPR profiles of Ru catalysts on different supports

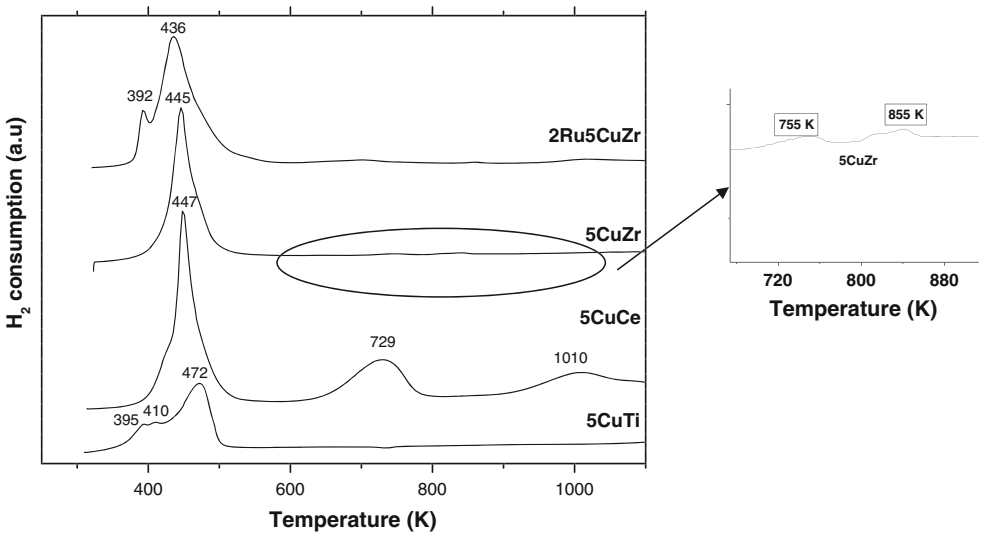

Fig. 3 TPR profiles of Cu catalysts on different supports

5CuZr. This could be due to the hydrogen spillover effect favored by the presence of ruthenium [24].

3.1.3 XPS Results

The Cu 2*p*, Ru 3*d* and 3*p*, Ti 2*p*, Ce 3*d* and Zr 3*d* core-levels of fresh and used catalysts, and the metal/supported intensity ratio are summarized in Table 1. The fresh catalysts were measured as calcined samples. In this table, the chemical state changes of Cu and Ru and their relative proportion on the support surface were showed for both fresh and used catalysts. The binding energies of the Cu $2p_{3/2}$ peak for fresh samples are in a close range (933.7–934.2 eV). These values can be assigned to Cu^{2+} species [25, 26]. Some decrease of the binding energy for copper catalysts after reduction and reaction was observed in this Cu $2p_{3/2}$ level. According to this, peak in the range between 932.7 and 932.8 eV, part of the copper seems to be in its metallic state after their use under partial oxidation reaction [25]. This effect can be observed in the 5CuZr catalyst. The catalysts analyzed after their use in *n*-butanol partial oxidation reaction showed one additional peak of Cu^{2+}. The Cu^{2+} peak is accompanied by a shake-up satellite line positioned at 8 eV higher BE, characteristic of Cu^{2+} ions. Hence, in oxidation conditions to peaks were detected on the catalytic surface: Cu^{0} and Cu^{2+}. Hence, after the studied condition some oxidation of metallic Cu occurred. For the fresh catalysts, the Zr 3*d* energy level took a value between 181.7 and 182.1 eV corresponding to ZrO_2 [26], and in the case of the Ti 2*p*, the values registered at 458.6–458.7 eV can be assigned to the presence of typical Ti^{4+} (TiO_2). The Zr spectra were unchanged after its use in reaction. The 5CuTi presented the highest surface copper support atomic ratio, and the 5CuZr presented the lowest copper/support atomic ratio at fresh conditions. After being used in reaction, the Cu/Zr ratio decreased with

respect to the fresh catalyst. In copper catalytic systems, the Cu/M ratio was close or higher than bulk one. This can be related with the high deposition of copper on the outer surface of titania or zirconia support.

For ruthenium catalysts, the Ru $3d_{5/2}$ level was analyzed. According to literature [27–29] the Ru $3d_{5/2}$ core-level can show different binding energies in the ranges of 279.9–280.7, 280.7–281.0, 281.7–282.6 and 282.6–283.3 eV that can be ascribed to Ru^0, RuO_2, RuO_3, and RuO_4, respectively. Hence, it seems that different Ru oxides and ruthenium metallic species were present in ruthenium catalysts. After their use in reaction, less intense Ru $3p_{3/2}$ peaks were measured since the Ru 3*d* component overlapped with the C 1*s* components. In addition to this, it was very complicate to assign a fix value to Ru signal in the 2RuCe catalyst. For the 2RuZr the peak centered at 461.5 eV can be assigned to metallic ruthenium and the peak situated at 462.5 eV corresponds to RuO_2 [30]. The Ru^{4+} species can be derived from oxidation under the reaction conditions. Finally, in the 2RuTi used catalyst only metallic ruthenium was detected. Regarding the surface Ru/support atomic ratio, at fresh conditions the 2RuZr showed the highest ruthenium dispersion on the support surface. The second one was the catalyst supported on ceria. Finally, the catalyst with the lowest ruthenium dispersion was the catalyst supported on titania. As in previous results the Ru/M bulk ratio was lower than measured ones, this can be related to the ruthenium preferent deposition on the outer support surface. After reaction, the ruthenium dispersion on the surface decreased for all the ruthenium catalysts as compared to fresh catalysts. In the case of 2RuTi and 2RuCe this dispersion reduction was extremely high. The surface ruthenium reduction for 2RuTi was around the 80.4 %, and in the case of the 2RuCe was over 83.5 % as measured by XPS. For the 2RuZr, the ruthenium surface reduction was approximately 25.8 %.

For the Ru–Cu fresh bimetallic system, the behavior was very similar to the one of monometallic systems. For the 2Ru5CuZr fresh calcined catalyst two different ruthenium species were detected, RuO_2 and RuO_4 [29] with values of binding energies of 281.0 and 282.9 eV, respectively. Regarding to copper, the binding energy of 934.2 can be assigned to Cu^{2+} [25] in the 2Ru5CuZr fresh catalyst. For the used 2Ru5CuZr catalyst, new peaks of copper were detected at 933.7 and at 936.3 eV. The peak at 933.7 eV corresponds to Cu^{2+} [25, 26] and the peak situated at 936.2 eV could be assigned to Cu^{2+} strongly interacting with the support. After the reduction or after its use in reaction, this catalyst suffered both reduction and oxidation processes. Regarding the ZrO_2 support, a new phase of Zr was detected by XPS. This new peak of Zr detected at 180.1 eV could be due to the reduction of the ZrO_2 to metallic zirconium [31]. For the ruthenium and copper atomic support ratio, the fresh bimetallic system presents higher ruthenium and copper dispersions on the ZrO_2 support than the monometallic ones. In addition, in this case of the measured Ru or Cu/Zr ratio were also higher than bulk ratios. After reaction, this effect was maintained for the copper, but no for the ruthenium: the surface copper/support atomic increased as compared to the equivalent values for the fresh catalyst, and the surface ruthenium/support ratio decreased.

3.1.4 XRD

As it was reported in our previous work [32], where part of these catalysts were tested in another reaction, the XRD patterns showed that the catalysts contained different crystal species. For the reduced $5Cu/TiO_2$ catalysts reflexions associated to Cu^0 (PDF 01-085-1326) and anatase and rutile type TiO_2 (PDF 01-071-1166 and 01-075-1750 respectively) were detected [32]. In the case of the reduced $5Cu/ZrO_2$ catalyst only ZrO_2 reflexions (PDF 01-079-1771) were registered. In addition, the absence of any Cu^0 signal was indicative of a good dispersion of this Cu on ZrO_2 support [32]. In the case of the reduced $2Ru5Cu/ZrO_2$ catalyst no reflexions of Ru and Cu phases were observed suggesting good dispersion of metal phases [32]. Finally, the reduced $5Cu/TiO_2$ catalysts presented an average Cu^0 particle of 51.4 nm [32].

3.2 Catalysts Activity

The main C4+ products derived from the activity test carry out were butyraldehyde, and other by-products such as *n*-dibutyl-ether, *n*-butylbutyrate and 4-heptanone. Traces of other condensation by-products were also detected, but their concentrations were very low so they were despised. As light by-product hydrogen, and other compounds such as CO, CO_2, CH_4, and saturated and unsaturated hydrocarbons (C3 and C4) were identified.

In order to analyze the effect of metallic phase and catalyst support, the activities of the different catalysts are compared after 2 (Fig. 4a) and 27 (Fig. 4b) hours on stream. Figure 4 a and b show the product yields obtained. The yields to *n*-dibutyl ether and 4-heptanone are presented combined as C7 + C8. The behaviour all of the catalytic systems were rather similar. At the beginning of the activity test low quantities of 4-heptanone and dibutyl-ether were detected. After 27 h on stream these compounds were not detected and the *b*-butylbutyrate selectivity was the most important contribution. As a result for times on stream larger than 27 h C7 + C6 yield and butyraldehyde yield are almost the same. This clarification has been included in the new version. According to the results, both the support and the metallic phase influenced on both

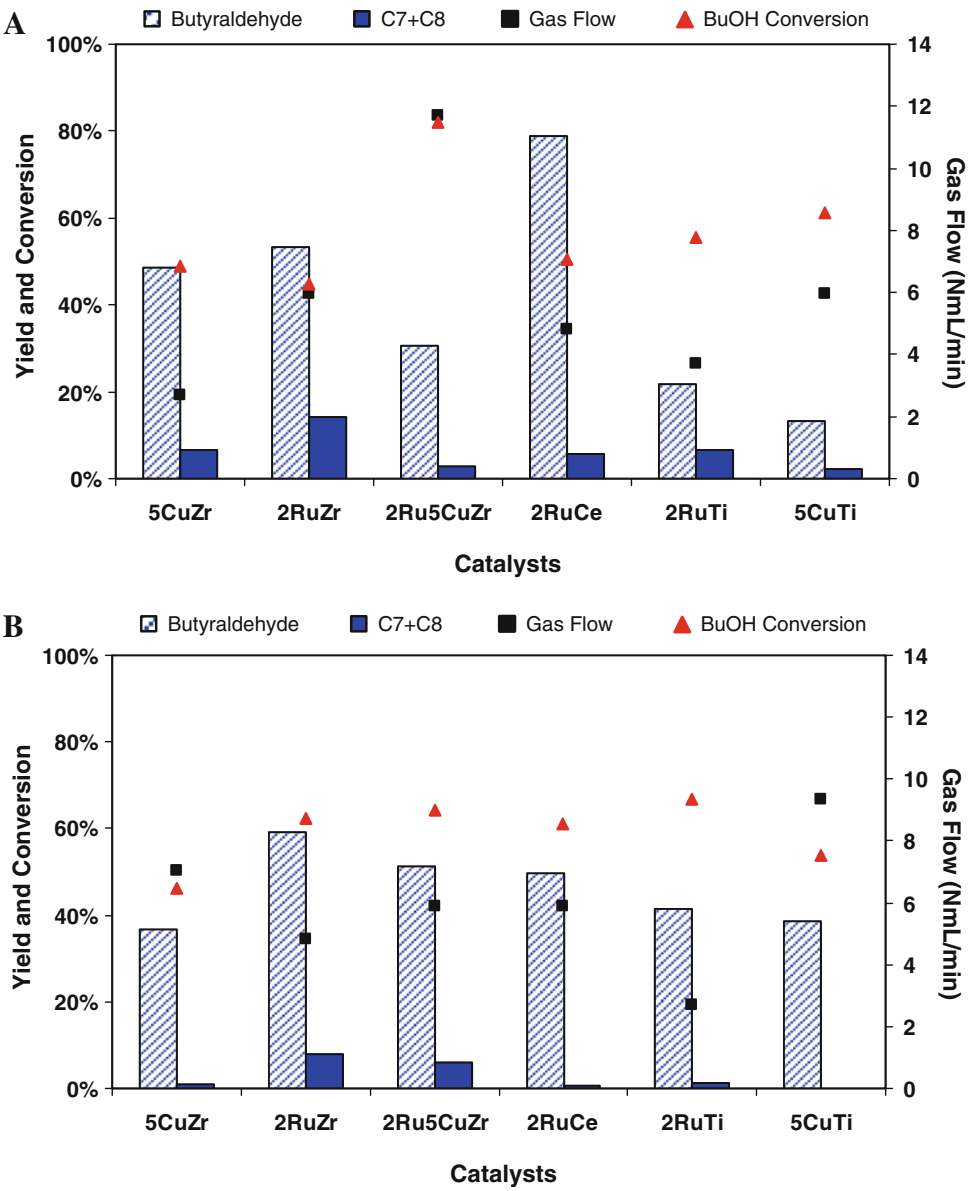

Fig. 4 BuOH conversion, total gas flow produced and yields in liquid stream **a** at 2 h on stream **b** at 27 h on stream

conversion and reaction yields. Under the conditions studied, the ruthenium catalysts showed the highest *n*-butanol conversion, around 62–66 %, after 27 h on stream (Fig. 4b). The *n*-butanol conversion was almost similar for all ruthenium catalysts. At the first hours on stream the *n*-butanol conversion (Fig. 4a) was lower than at 27 h on stream, and for times on stream higher than 7 h the performance remained stable. For higher times on stream the 2RuZr, and 2RuTi allowed higher butyraldehyde yields while condensation by-products decreased. This same behavior was shown by the 2RuCe system, but its butyraldehyde yield decreased with time on stream. This lower butyraldehyde yield was in agreement with a higher light compounds production. Furthermore, the 2RuZr and 2RuCe catalysts showed the best yields towards butyraldehyde production, followed of 2RuTi catalyst. Ruthenium catalyst supported on ZrO_2 showed a greater tendency towards the formation of condensation products, associated to a lower light compounds formation, while the quantities produced by the rest of the catalysts were very low. The 2RuCe catalyst after 2 h on stream presented the highest butyraldehyde yield (close to 80 %), but for higher hours on stream, the butyraldehyde yield decreased and the gas by-produced increased. The 2RuTi was the catalyst which the highest *n*-butanol conversion, but the catalyst producing the lowest butyraldehyde yields; this can be explained analyzing the gas composition of the gas generated. The gas flow produced was the lowest due to its composition, rich in C3–C4 saturated and unsaturated hydrocarbons. On the whole, the presence of Ru in the

catalysts decreased the gas flow obtained and modified the gas composition. TA higher gas flow of these catalysts indicates higher contents of CO_2, H_2, and CO, while a lower gas flow indicates higher contents of hydrocarbons such as C_3H_8, C_3H_6, C_4H_{10} and C_4H_8. The presence of Ru in the catalyst favoured the presence of short paraffin and olefin products in the gas stream. For example, for the 2RuZr, 2RuTi and 2RuCe the main product in the gas stream was CO_2 and the presence of hydrocarbons could be confirmed. These hydrocarbons were C_3H_8, and C_3H_6. In the case of the 2RuTi, C_4H_{10} and C_4H_8 were also detected. Hence, even if the 2RuTi presented the highest *n*-butanol conversion, its *n*-butyraldehyde and C7 + C8 yields, and its total gas-flow were lower due to the presence of significant amount of C_4H_8 and C_4H_{10} in gas phase.

Monometallic copper catalysts showed lower activities than the ruthenium and bimetallic ones. Among monometallic copper catalysts, the best performance was measured for the 5CuTi catalyst: 55 % conversion after 27 h, while for the 5CuZr *n*-butanol conversion was approximately 46 %. For both copper catalysts, the stability was similar, although the 5CuZr started with higher conversions (Fig. 4a, b). After the initial deactivation, for zirconia supported catalyst the activity remained almost stable under reaction conditions. It is remarkable that during the time on stream for the 5CuZr catalyst the butyraldehyde, *n*-butyl-ether and 4-heptanone yields decreased, while the total gas flow increased (light product). For the 5CuTi the behavior was different, the total gas flow also increased, the *n*-butyraldehyde yield increased and the C7 + C8 product decreased. In this case, the copper catalysts supported on ZrO_2 also showed a greater tendency towards the formation of condensation products, while the quantities produced by the 5CuTi catalyst were insignificant. Nevertheless, comparing the result of butyraldehyde yield, the ruthenium catalysts presented higher butyraldehyde yield than the measured for the monometallic copper ones. As it can be observed in Fig. 4a and b, the gas production was very high for the monometallic copper catalysts (5CuZr and 5CuTi). The main gas by-products obtained with these catalysts were H_2 and CO_2, and no hydrocarbons were detected.

The bimetallic 2Ru5CuZr supported catalyst showed a good activity in this type of reaction. After 27 h on stream, the conversion reached was a little bit higher than the one reached by the ruthenium monometallic catalyst supported on ZrO_2: 64.3 %. The catalyst activity of 5CuZr improved substantially with the incorporation of ruthenium: 2Ru5CuZr. As 5CuZr catalyst, the 2Ru5CuZr catalyst started with higher conversions for the first hours (79 % of *n*-butanol conversion, Fig. 4a, b). After an initial deactivation, its activity remained almost stable under reaction conditions after 27 h on stream. The 2Ru5CuZr showed higher activity than 2RuZr, and 5CuZr, but an intermediate selectivity to butyraldehyde between those obtained using: 2RuZr and 5CuZr: 2RuZr > 2Ru5Cu Zr > 5CuZr (Fig. 4b). The bimetallic catalyst reduced the butyraldehyde selectivity and also the condensation products. Regarding the condensation by-products, as 5CuZr and 2RuZr, the presence of ZrO_2 increased this by-products yield. For the bimetallic catalyst the yield towards condensation products was slightly lower than the one obtained using 2RuZr, but higher than the one of the catalyst 5CuZr. The copper presence increased light products avoiding condensation products. The gas composition of this last catalyst had a similar behaviour than the one showed for 2RuZr catalyst, but lower amounts of C_3H_8 and C_3H_6 were obtained. Finally, it is remarkable that during the time on stream for the 2Ru5CuZr the total gas flow decreased and the C7–C8 yields increased.

4 Discussion

The activity and yield of the copper catalysts were different depending on the support used. The copper TiO_2 supported catalyst presented higher activity and stability than the ones showed by the copper ZrO_2 supported one. The copper dispersion on the catalyst surface of the ZrO_2 was lower for ZrO_2 than for the TiO_2 (XPS). Nevertheless, the copper content of the 5CuZr was higher than the one of the 5CuTi (ICP-AES). This could indicate that part of the copper was incorporated inside the zirconia structure, and this copper incorporated to ZrO_2 structure was not active in the *n*-butanol oxidation process. The high porosity of the zirconia (BET) could help this copper incorporation into the zirconia structure. A higher copper dispersion on the catalyst implied higher activity. After reaction, the copper dispersion on the surface was lower for the 5CuZr and part of the copper on the external surface was oxidized (XPS), hence some deactivation took place in this catalyst due to metallic copper loss on external surface. This is coherent with the activity lowering measured. For the copper catalyst supported on TiO_2 the behaviour was different. No deactivation was observed, hence it is probable that no sinterization took place on the catalytic surface due to a higher interaction between the support and the active metal than in the case of the 5CuZr (TPR). Regarding the butyraldehyde selectivity, this was higher for the 5CuZr catalyst than for the 5CuTi, although the *n*-butanol conversion was higher for the 5CuTi. This effect was due to a higher oxidation of *n*-butanol to CO_2 and H_2 when using 5CuTi than when 5CuZr was used; hence the gas flow obtained with 5CuTi was higher than with 5CuZr. In addition, the presence of ZrO_2 increased this by-products yield. This effect could be attributed to the basic nature of the zirconia support, which

favoured the condensation/oligomerization reactions [33, 34].

All ruthenium catalysts showed a high activity and stability in the partial oxidation from *n*-butanol to butyraldehyde. The ICP-AES data showed that the ruthenium content was similar in these catalysts. The total pore volume reduction in the ZrO_2 and TiO_2 support after the ruthenium incorporation (BET) indicates that the ruthenium incorporation was mainly on the support outer surface. These data are in good agreement with the dispersion measured by XPS. However, it seems that the initial dispersion of ruthenium (XPS) have no influence in the activity, but it influenced the butyraldehyde yield. The higher initial dispersion was obtained for the 2RuZr, and the lower dispersion was measured for 2RuTi, while the 2RuCe presented as an intermediate ruthenium dispersion (XPS). The 2RuTi catalyst reached the highest *n*-butanol conversion and its stability was quite high after the highest time on stream (27 h), but the butyraldehyde yield was lower for 2RuCe and 2RuZr. Using the 2RuZr catalyst (the catalysts with the highest metal dispersion) higher butyraldehyde yield after 27 h on stream was obtained. This catalyst also presented the highest condensation by-products production (Fig. 4a, b). As all of catalysts supported on ZrO_2, this result was due to the condensation/oligomerization reactions being favoured by the ZrO_2 presence. After reaction all monometallic ruthenium catalysts lost ruthenium surface (XPS). The monometallic catalyst with the minimum ruthenium dispersion loss was 2RuZr, while the 2RuTi and 2RuCe presented higher ruthenium dispersion losses. Nevertheless, no activity decay was observed during the time on stream for any of these catalysts. In addition to Ru particles sinterization, it is possible that some volatile metal oxides formation also occurred: metal crystallite stability depends on the volatility of metal oxides and the strength of the metal oxide–support interaction, so the formation of volatile RuO_4 accounts for the relative instability of ruthenium [35]. But, it seems that the presence of small ruthenium amounts on the catalyst surface is enough to maintain high activities in the *n*-butanol partial oxidation to produce butyraldehyde.

The bimetallic 2Ru5CuZr supported catalyst showed a good activity in this type of reaction. This bimetallic catalyst reduced the butyraldehyde selectivity and also the condensation products with respect to 2RuZr. It seems clearly that the copper hydrogenation and dehydrogenation activity help avoiding these condensation products. For the 2Ru5CuZr catalyst the ruthenium dispersion after reaction was lower than the one measured for the fresh (no reduced) catalyst, but at the same time, the copper amount on the catalytic surface was higher than on the fresh catalyst (XPS). It seems that after reduction and its use in *n*-butanol oxidation some changes took place in the support. This changed could take place due to the reduction of ZrO_2 to metallic zirconium (XPS, TPR). This phenomenon had a high initial influence in the activity of this catalyst as compared to the ruthenium and copper monometallic catalysts. The conversion was very high along the first hours (79 % of *n*-butanol conversion at 2 h). Even though, after 27 h the activity decreased along the time on stream (64.3 % of *n*-butanol conversion). The initial high conversion was due to the high dehydrogenation capacity of this catalyst that can be related to the production of high amounts of gas-flow rich in H_2 and CO_2. During the time on stream this dehydrogenation capacity decreased and the heavier products generation increased with respect to those appearing in gas phase.

5 Conclusions

Ruthenium catalysts supported on ZrO_2, TiO_2, CeO_2 and ruthenium–copper catalyst supported on ZrO_2 were found to exhibit promising activities and stability for the *n*-butanol air partial oxidation to butyraldehyde in gas phase. Hence, this new route of n butyraldehyde production seems to be a new promising alternative.

The copper metallic catalysts supported on ZrO_2 and TiO_2 presented lower activities than the ruthenium ones. The 5CuTi catalyst presented higher activity and stability than 5CuZr. These results can be related to a possible incorporation of the copper to non accessible areas on the ZrO_2 structure.

Ruthenium incorporation to 5CuZr catalyst highly increased the conversion and the stability of the catalyst as compared to the corresponding Cu monometallic catalyst. The presence of Cu in this bimetallic catalyst improved the selectivity towards butyraldehyde.

Acknowledgments The authors gratefully acknowledge the financial support of this work by the Spanish Ministry of Innovation and Science ENE2009-12743-C04-04, and the University of the Basque Country UPV/EHU.

References

1. Cornils B, Fischer RW, Kohlpaintner C (2000) Ullmann's encyclopedia of industrial chemistry. Wiley-VCH, Weinheim
2. Kohlpaintner CW, Fischer RW, Cornils B (2001) Appl Catal A Gen 221:219–225
3. Sheldon RA, Arends IWCE, Dijksman A (2000) Catal Today 57:157–166
4. Marko IE, Giles PR, Tsukazaki M, Chell′e-Regnaut I, Gautier A, Dumeunier R, Philippart F, Doda K, Mutonkole J-L, Brown SM, Urch CJ (2004) Adv Inorg Chem 56:211–240
5. Sheldon RA, Arends IWCE, Ten Brink G-J, Dijksman A (2002) Ace Chem Res 35:774

6. Kockritz A, Sebek M, Dittmar A, Radnik J, Brückner A, Bentrup U, Pohl M–M, Hugl H, Magerlein W (2006) J Mol Catal 246:85–99
7. Magaeva AA, Lyamina GV, Sudakova NN, Shilyaeva LP, Vodyankina OV (2007) Chem Kinet Catal 81:1613–1617
8. Gilhespy M, Lok M, Baucherel X (2005) Chem Commun 8:1085–1086
9. Rajabi F, Karimi B (2005) J Mol Catal A Chem 232:95–99
10. Naik R, Joshi P, Deshpande RK (2004) Catal Commun 5:195–198
11. Caravati M, Grunwaldt JD, Baiker A (2004) Catal Today 91(92):1–5
12. Shapley PA, Zhang N, Allen JL, Pool DH, Liang H-C (2000) J Am Chem Soc 122:1079
13. Shiau CY, Liaw ST (1992) J Chem Technol Biotechnol 53:13–19
14. Basinska A, Klimkiewicz R, Domka F (2001) Appl Catal A Gen 207:287–294
15. Raizada VK, Tripathi VS, Lal D, Singh GS, Dwivedi CD, Sen AK (1993) J Chem Technol Biotechnol 56:265–270
16. Parentis ML, Bonini NA, Gonzo EE (2001) React Kinet Catal Lett 72(2):303–308
17. Iriondo A, Güemez MB, Requies J, Barrio VL, Cambra JF, Arias PL, Fierro JLG (2010) Stud Surf Sci Catal 175:453–456
18. Adam F, Andromena I (2009) J Porous Mater 16:321–329
19. Mitsui T, Tsutsui K, Matsui T, Kikuchi R, Eguchi K (2008) Appl Catal B Environ 81:56–63
20. Zonetti P, Landers R, Gomez Cobo AJ (2008) Appl Surf Sci 254:6849–6853
21. Reyes P, Köning ME, Pecchig G, Granados ML, Fierro JLG (1997) Catal Lett 46:71
22. Caputo T, Lisi L, Pirone R, Russo G (2008) Appl Catal A Gen 348:42–53
23. Shimokawabe M, Asakawa H, Takezawa N (1990) Appl Catal 59:45–58
24. Li L, Qu L, Cheng J, Li J, Hao Z (2009) Appl Catal B Environ 88:224–231
25. Ritzkopf I, Vukojevic S, Weidenthaler C, Grunwaldt J-D, Schüth F (2006) Appl Catal A Gen 302:215–223
26. Kundakovic Lj, Flytzani-Stephanopoulos M (1998) Appl Catal A Gen 171:13–29
27. Requies J, Rabe S, Vogel F, Truong TB, Filonova K, Barrio VL, Cambra JF, Güemez MB, Arias PL (2009) Catal Today 143:9–16
28. Ma L, He D, Li Z (2008) Catal Comm 9:2489–2495
29. John FM, William FS, Peter ES, Kenneth DB (1995) Handbook of X-ray photoelectron spectroscopy. Physical Electronics, Inc., Eden Prairie
30. Chan HYH, Takoudis CG, Weavery MJ (1997) J Catal 172: 336–345
31. Barr TL (1978) J Phys Chem 82(16):1801–1810
32. Torres G, Apesteguía CR, Di Cosimo JI (2007) Appl Catal A Gen 317:161–170
33. Requies J, Güemez MB, Iriondo A, Barrio VL, Cambra JF, Arias PL (2012) Catal Lett. doi:10.1007/s10562-011-0725-9
34. Bartholomew CH (2001) Appl Catal A Gen 212:17–60
35. Takanabe K, Aika K-i, Seshan K, Lefferts L (2006) Chem Eng J 120:133–137